Martian Equatorial Atmospheric Tides from Surface Observations

Joonas Leino[1], Ari-Matti Harri[1], Donald Banfield[2], Manuel de la Torre Juarez[3], Mark Paton[1], Jose Antonio Rodríguez-Manfredi[4], Mark T Lemmon[5], and Hannu Savijärvi[6]

[1]Finnish Meteorological Institute
[2]Cornell
[3]Jet Propulsion Laboratory- California Institute of Technology, Pasadena, CA, USA
[4]Centro de Astrobiología
[5]Space Science Institute
[6]University of Helsinki

October 9, 2023

Martian Equatorial Atmospheric Tides from Surface Observations

Joonas Leino[1], Ari-Matti Harri[1], Don Banfield[2], Manuel de la Torre Juárez[3], Mark Paton[1], Jose-Antonio Rodriguez-Manfredi[4], Mark Lemmon[5],Hannu Savijärvi[1,6]

[1]Finnish Meteorological Institute, Helsinki, Finland
[2]Cornell University, Cornell Center for Astrophysics and Planetary Science, Ithaca, NY, USA
[3]Jet Propulsion Laboratory/California Institute of Technology, Pasadena, CA, USA
[4]Centro de Astrobiologia (INTA-CSIC), Madrid, Spain
[5]Space Science Institute, Boulder, CO, USA
[6]Institute for Atmospheric and Earth System Research, Helsinki, Finland

Key Points:

- We analyze diurnal and semi-diurnal atmospheric tidal components from simultaneous InSight and Mars Science Laboratory observations
- We find higher amplitude of the diurnal harmonic component at Mars Science Laboratory location due to differences in topography
- We find a similar response between the harmonic components and atmospheric dust loading on both platforms

Corresponding author: Joonas Leino, `joonas.leino@fmi.fi`

Abstract

Diurnal solar radiation causes global oscillations in pressure, temperature, and wind fields, known as atmospheric tides, which are further modified by topography, surface properties, and atmospheric dust loading. Hence, the tides are a combination of sun-synchronous and non sun-synchronous tides that propagate around the planet both eastward and westward. In the Martian tropics, atmospheric tides dominate daily pressure variations on the surface. Therefore, surface observing platforms are extremely useful for detailed analysis of atmospheric tides. In this investigation, we analyze diurnal and semi-diurnal components of atmospheric surface pressure measured by the simultaneously operating InSight and Mars Science Laboratory (MSL) payloads. We utilize observations of the time period from Martian year 34 solar longitude 296° to Martian year 36 solar longitude 53°. The diurnal tide average amplitude is 17 Pa with an average phase of 03:39 local true solar time (LTST), while the semi-diurnal tide average amplitude and phase are 7 Pa and 09:34 LTST for the InSight. The corresponding values for the MSL are 33 Pa with 04:25 LTST for the diurnal and 10 Pa with 09:36 LTST for the semi-diurnal component. Thermo-topographic lateral hydrostatic adjustment flow generated by topography causes the higher diurnal amplitude observed by MSL. Both platforms observe a similar response between these harmonic components and dust loading. Furthermore, amplitudes obtained from a Mars Climate Database mimic the observations well. Our study provides for the first time a comparison of atmospheric tides at two simultaneously observing tropical surface platforms for more than one Martian year.

Plain Language Summary

The Curiosity rover landed on Mars in August 2012 and has been observing meteorological variables ever since. The next surface observing station, the InSight lander, landed in the equatorial region of Mars in November 2018, relatively close to Curiosity. Unfortunately, InSight reached end of its mission on December 15, 2022, but fortunately they observed Martian atmosphere simultaneously for more than one Martian year. Atmospheric pressure is a very important meteorological variable, since many weather phenomena are associated with changes in surface pressure. Here we use pressure observations from these two weather stations to determine Martian equatorial atmospheric tides and compare them with model simulations. They are forced by solar radiation and additionally modified by topography, surface properties, and atmospheric dust. They propagate around the planet in periods that are integer fractions of a Martian day. The two strongest components, diurnal and semi-diurnal, with periods of 24 and 12 hours, are studied here. The results show the effect of atmospheric dust loading and the location on these components. We find a similar response between these components and atmospheric dust loading on both platforms and a higher amplitude of the diurnal tide at the Curiosity location due to differences in topography.

1 Introduction

Atmospheric tides are the dynamical response to the diurnal heating of the atmosphere by the absorption of solar radiation and the daily heat flux from the surface. Thus, they are also called thermal tides, which can be detected as global oscillations in pressure, temperature, and wind fields. In addition to thermal forcing, they are modified by topography and surface properties. Atmospheric tides represent a very large part of the Martian atmospheric circulation (e.g. Zurek, 1976; Hamilton, 1982; Wilson & Hamilton, 1996; Banfield et al., 2000), on Earth, these tides are only relevant in the upper atmosphere (e.g. Hagan & Roble, 2001). The tidal differences between Earth and Mars are due to a difference of approximately two-orders of magnitude in the total column mass of the atmosphere. It is therefore important to characterize the atmospheric tides on Mars and there are a number of useful pressure observations made at different places on Mars that can help with this.

Theoretically, atmospheric tidal oscillations, so-called Hough function solutions are obtained from the Laplace's tidal equation, which is derived from the primitive equations that are linearized about a motionless basic state (Chapman & Lindzen, 1970). The Hough function solutions cover the meridional structure and a vertical structure equation can be solved for each of these solutions separately. The vertical structure equation is a second-order equation, including heating as an inhomogeneous term.

Atmospheric tides propagate around the planet in periods that are integer fractions of a solar day. A single atmospheric tide (e.g. diurnal) can be further divided into westward propagating sun-synchronous and either eastward or westward propagating non sun-synchronous waves. These can be further divided into modes that respond differently to forcing mechanisms due to their unique meridional and vertical structure. Therefore, each tide is a combination of several Hough function solutions.

The lowest-order Hough function solution of the sun-synchronous diurnal tide is insensitive to atmospheric dust loading at high latitudes, since it is equatorially-trapped (e.g. Chapman & Lindzen, 1970; Wilson & Hamilton, 1996). This mode is more sensitive to local vertical distribution of dust due to its small vertical wavelength, which is approximately 32 km. However, the lowest-order Hough function solution of the sun-synchronous semi-diurnal tide has a long vertical wavelength (100–200 km) and is meridionally-broad (e.g. Chapman & Lindzen, 1970; Wilson & Hamilton, 1996; Bridger & Murphy, 1998). Therefore, this mode is sensitive to global atmospheric dust loading.

Theoretical calculations suggest that the sun-synchronous semi-diurnal tide at a given surface location is largely represented by the lowest-order Hough mode, described above, while the sun-synchronous diurnal tide is a combination of several Hough modes (Chapman & Lindzen, 1970). Nonetheless, each harmonic component, e.g. diurnal and semi-diurnal tide, is a combination of sun-synchronous and non sun-synchronous tides.

The airborne dust in the Martian atmosphere acts as an effective absorber (e.g. Savijärvi et al., 2005) and thus significantly affects atmospheric tides (e.g. Zurek, 1976; C. Leovy & Zurek, 1979; C. B. Leovy, 1981; Wilson & Hamilton, 1996; Bridger & Murphy, 1998; Guzewich et al., 2016). In addition to atmospheric dust loading, Martian topography has a significant effect on the tides, generating both eastward and westward propagating waves with different zonal wavenumbers (Wilson & Hamilton, 1996). Wilson and Hamilton (1996) studied extensively diurnal and semi-diurnal pressure oscillations in the Martian atmosphere using a general circulation model and Viking lander observations. Their results suggest that the diurnal pressure oscillation has a zonal wavenumber 2 structure, resulting from the interference of eastward (i.e. diurnal Kelvin wave) and westward propagating zonal wavenumber 1 components. The semi-diurnal tide, however, has a zonal wavenumber 4 pattern, resulting from the interference of eastward (i.e. semi-diurnal Kelvin wave) and westward propagating zonal wavenumber 2 components.

Guzewich et al. (2016) studied atmospheric tides in Gale Crater, which is located near the equator. They analyzed the tides using Mars Science Laboratory (MSL) pressure observations for more than one Martian year and the Mars Weather Research and Forecasting Model (MarsWRF) general circulation model (GCM). Their results suggest that both diurnal and semi-diurnal tides are highly correlated with atmospheric opacity variations. In addition to this, they found that the diurnal Kelvin wave amplifies the amplitude of the diurnal tide, while the semi-diurnal Kelvin wave slightly weakens the semi-diurnal tide within the Gale Crater.

To our knowledge, atmospheric tides are not studied in detail at the InSight location. In this study, we focus on analyzing the atmospheric tides from the InSight pressure observations and compare them with Mars Science Laboratory (MSL) observations.

It would be advantageous, if more simultaneously operating observation sites would be available (Squyres, 1995; Harri et al., 1999). Using InSight and MSL pressure observations we compare, for the first time, atmospheric tides on two simultaneously observing tropical surface platforms over more than one Martian year. In Section 2, we present the InSight and MSL pressure observations and describe both data sets. The data analysis at both locations together with the results from the Mars Climate Database are shown in Sections 3 and 4. The results are summarized and discussed in Section 5.

2 Observations

The Mars Science Laboratory (MSL) Curiosity rover has been measuring meteorological variables within Gale Crater (4.6 °S, 137.4 °E) for more than five Martian years (MY). The rover includes Rover Environmental Monitoring Station (REMS, Gómez-Elvira et al., 2012) which measures, among other quantities, air pressure (Harri et al., 2014) typically in 5-minute blocks every hour, but occasionally it also measures extended, usually one-to-three-hour blocks. Together with REMS pressure observations, we use here dust optical depth measurements by Mastcam (Lemmon, 2014), since thermal tides are sensitive to the atmospheric dust loading (e.g. Wilson & Hamilton, 1996; Guzewich et al., 2016).

InSight landed on Mars on November 26, 2018 (MY 34 Ls 295°) a couple of Martian years later on Elysium Planitia (4.5 °N, 135.6 °E). Unlike MSL, InSight measured meteorological variables continuously at a high frequency (Spiga et al., 2018), which is extremely useful for detecting weather phenomena on different time scales. InSight's last communication was received on December 15, 2022 (MY 36 Ls 354°) and it managed to measure air pressure regularly for slightly over one MY.

In this study, we use so-called hourly data sets. For each sol, the pressure data was binned into one hour intervals based on local true solar time (LTST) and the averaged value represents the hourly value. The hourly data was then used to calculate the sol-averaged pressure. The average variation in pressure within an hour for MSL is between about 5 and 18 Pa, with the largest variations typically between 18 and 19 LTST. Sol-averaged pressure as observed by InSight (black) and MSL (blue) over MY 35 as a function of solar longitude (Ls) is demonstrated in Figure 1 (left panel). It also shows the sol-averaged pressure obtained from the Mars Climate Database (Forget et al., 1999; Millour et al., 2017) at both locations (green InSight, red MSL). The right panel of Figure 1 shows the diurnal range of pressure (minimum to maximum value relative to the average) over MY 35 from InSight (black) and MSL (blue) observations.

The annual sol-averaged pressure cycle is very similar on both observing platforms as well as the cycle obtained from MCD. The cycle is dominated by the annual exchange of CO_2 between the polar caps and is therefore smooth and repeatable. The differences in the absolute pressure values are due to the elevation difference between the two platforms. The elevation difference between the stations varied between 1405.54 and 1495.9 m during MY 35 (Vasavada et al., 2014; Karlgaard et al., 2021). This is demonstrated with the sol-averaged pressure from the MSL observations at the height of the InSight lander (solid blue). The pressure is obtained assuming hydrostatic condition with a scale height of 11 km. These yearly cycles match quite well but they also have some differences. These variations may be related to the scale height as it is a function of the column temperature, and therefore varies during the year. The MCD results are close to the InSight observations, but differ slightly from the MSL observations. This is most likely due to the fact that the InSight is located on a flat surface, while the elevation of the MSL has changed within the Gale Crater from about -4501 m at the beginning of the mission to -4019 m at the end of MY 35 (Vasavada et al., 2014). Also, local dust conditions may vary from the model and therefore may affect sol-averaged pressures. Furthermore, the difference between measurements and simulations is not constant. In particular, the match close to aphelion is almost perfect while MCD overestimates the pressure at perihelion. This may be related to atmospheric dust conditions, as there is greater dust activity during the perihelion season (Martínez et al., 2017). In the MCD, the high resolution surface pressure is obtained hydrostatically using a predicted temperature at about 1 km above the surface, which may vary from the real value. Since the airborne dust act as an effective absorber, the air temperatures and thereby also the surface pressures predicted by MCD may differ more from the observations during perihelion than aphelion season.

Right panel of Figure 1 shows very similar diurnal pressure range pattern over MY 35 on both surface platforms. Both observe minimum at about Ls 120° and two clear maxima at about Ls 230° and Ls 320°. In addition, the variations throughout the year in the relative diurnal pressure range between the stations are very small. Small differences, for example around Ls 150°, may be related to rapid changes in local dust conditions. However, the absolute and relative values of the diurnal range of pressure are much higher at the MSL location although it is located relatively close to InSight. The high diurnal pressure range at the MSL is caused by the combined effects of the synoptic-scale (> 500 km) thermal tide and the thermo-topographic lateral hydrostatic adjustment flow within the Gale (Richardson & Newman, 2018). The same does not apply for InSight, as it is located on a flat surface and the influence of topography on the diurnal range of pressure is much smaller.

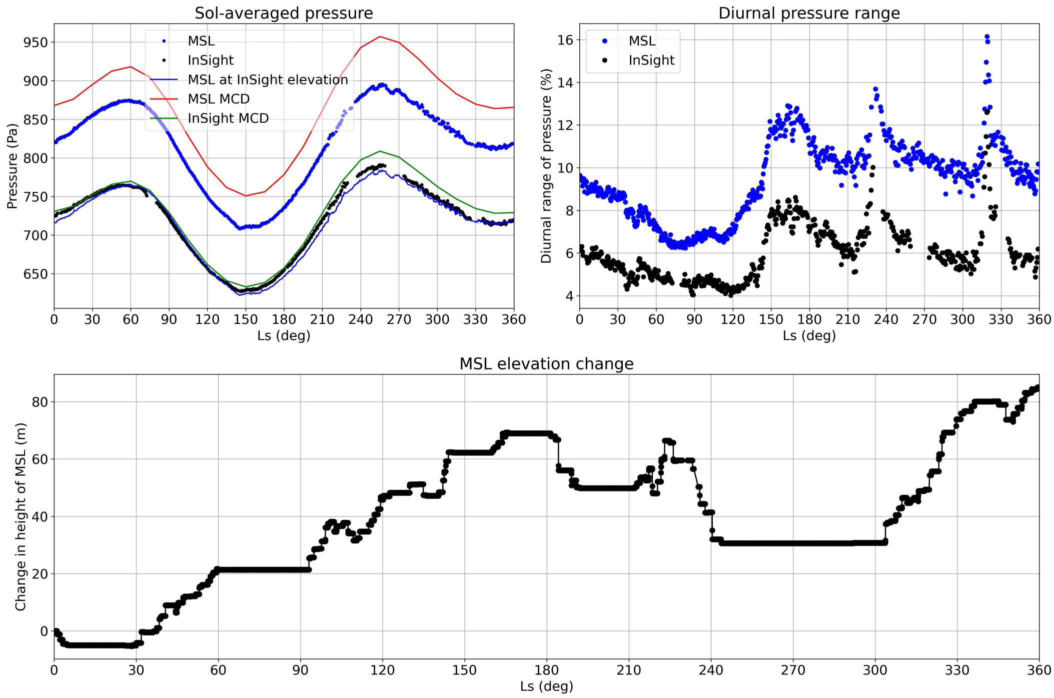

Figure 1. Upper left panel shows sol-averaged pressure (Pa) as observed by InSight (black) and MSL (blue) over MY 35. Sol-averaged pressure from MCD at the locations of InSight (green) and MSL (red) are also shown. In addition, sol-averaged pressure from the MSL at the elevation of InSight (solid blue) is shown. Upper right panel displays diurnal range (minimum to maximum value relative to the average) of pressure as observed by InSight (black) and MSL (blue). Lower panel shows the change in height of MSL during the MY 35.

To further investigate atmospheric tides, we use a fast Fourier transform (FFT) approach. In the present investigation, we first used a window of three sols, where amplitudes and phases were calculated for the middle sol. The daily mean was first subtracted from the hourly data of the three sol window. The average for each perturbed hour was then calculated and used as an input to the FFT. This approach assumes that the three consecutive sols in each window are similar enough to calculate the largest harmonic components. This approach was used to make sure that we would get 24 data points for as many sols as possible. Thereafter, to make the MCD data and observational sol data quite similar, we changed the moving window to one sol. This change did not cause any apparent changes compared to using a window of three sols. The original pressure signal $p(t)$ can then be calculated from Equation 1:

$$p(t) = p_0 + \sum_k P_k \cos(\omega_k t + \theta_k), \tag{1}$$

where p_0 is the sol-averaged pressure, P_k is the amplitude of the harmonic component, ω_k is the angular frequency of the component, t is local true solar time (LTST), and θ_k is the phase of the harmonic component. A similar approach is used for the surface pressures obtained from the MCD.

Due to uneven MSL observations (see Section 3), the hourly binned data in the FFT analysis causes some uncertainty when calculating amplitudes and phases because we assume the timestamp in the middle of each hour. The InSight lander, however, generally measured continuously. Therefore this approach is more accurate for the InSight measurements. We estimate this uncertainty for the MSL with a Monte Carlo analysis using a five sol window to divide the data into hourly bins. Then the uncertainty in pressure is approximated within each hour as a half of the difference between the maximum and minimum. This uncertainty was then multiplied by a uniform distribution between -1 and 1 and added to an original hourly data of the sol. Total of 500 different diurnal pressure cycles were drawn around the measured cycle for each sol and used as an input for the FFT. This way the approximate maximum uncertainty is taken into account.

3 General Observed Pressure Features from InSight and MSL

Figure 2 shows the diurnal pressure evolution during MY 35 for the InSight (lower pressures in each panel) and MSL (higher pressures in each panel). They cover the full year in steps of Ls 45°, each panel (a, b, c, d, e, f, g, and h) contains five sols, with the middle sol (red) roughly corresponding to the Ls value above the Figure. These panels clearly show that the InSight measured continuously, except for some data gaps (e.g. Figures 2 f and g), while the MSL generally measured short blocks, with some extended blocks.

Two maxima in the annual sol-averaged pressure cycle (Figure 1) can also be detected from the both diurnal pressure cycles. For both observing platforms, each Figure show local pressure maximum at 6–9 LTST and local minimum at 15–18 LTST. On top of that, another maximum can be seen at 18–21 LTST at Ls 0°, 90°, 135°, 180°, and 225°, slightly more clearly at the InSight's location compared to the MSL. Therefore, the diurnal pressure cycle at both equatorial weather stations is dominated by a wave with a period of 24 hours, which is also seen in the tide analysis in Section 4.

There are, however, some differences between the platforms. The diurnal pressure cycle within Gale (MSL) is more heavily dominated by the wave with a period of 24 hours, while the pressure cycle observed by the InSight includes additionally a more pronounced wave with a period of 12 hours. This is also displayed in the tide analysis in Section 4.

Since the two tropical weather stations have similar thermal forcing, the difference in the diurnal pressure cycles must be explained by other mechanisms. One difference between the stations is the topography. It causes a lateral hydrostatic adjustment flow

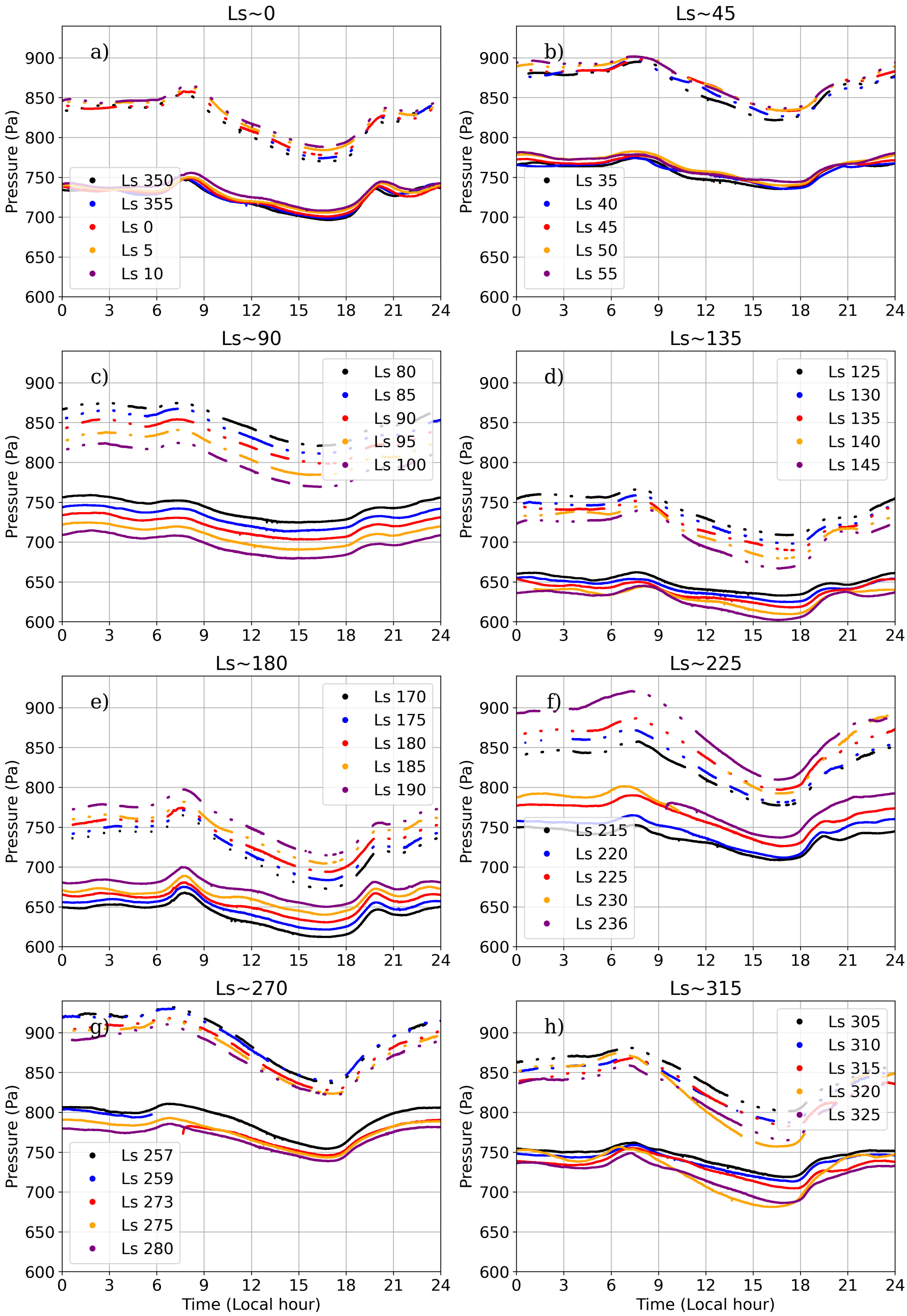

Figure 2. Evolution of MSL's (discontinuous line) and InSight's (continuous line) diurnal pressure cycles over MY 35. Each Figure shows data from five sols and the middle sol (red) roughly corresponds to the Ls value above each Figure.

at the MSL location, which increases the amplitude of the diurnal pressure range (Richardson & Newman, 2018). Local airborne dust is moreover one of the factors that may play a role here, since the surface pressure is sensitive to the local vertical distribution of dust.

In Figure 2, InSight's continuous measurements at high sampling rates reveal short-duration (< 100 s) pressure drops in the diurnal pressure cycles. These pressure drops are called dust devils or convective vortices, depending on whether they contain dust or not (e.g. Harri et al., 2014; Spiga et al., 2021). They get their energy from solar radiation and thus occur around midday.

4 Investigation of Simultaneous Insight and MSL Observations Using Semi-diurnal and Diurnal Tidal Component Analysis During the InSight Mission Time Period

The FFT analysis is performed during the period when the InSight measured pressure regularly. This roughly corresponds to MY 34 Ls 296° to MY 36 Ls 53° (InSight sols 1–894). The analysis is performed on the MSL pressure observations of the same period corresponding approximately to the MSL sols 2243–3136. A Martian year 35 dust scenario is used in the MCD results shown here. Results with a window of one sol are shown here.

The amplitude of the diurnal (black and orange) and semi-diurnal (blue and purple) components at both locations as a function of season (Ls) are shown in Figure 3 middle panel. In addition, the Figure show the components calculated from the MCD surface pressure (red and green for the MSL, gray and cyan for the InSight). The corresponding results for the diurnal and semi-diurnal phases are shown in the lower panel. In addition, upper panel of Figure 3 shows the Mastcam dust optical depth (gold) and daily mean dust column visible optical depth above surface from the MCD (purple).

Both stations clearly demonstrate the higher amplitude of the diurnal component compared to the semi-diurnal during this measurement period, which was also predicted in Section 3. Moreover, they show the sensitivity of the diurnal component to the local dust optical depth (Figure 3 upper panel), which is in good agreement with previous studies (e.g. Zurek, 1976; Wilson & Hamilton, 1996; Guzewich et al., 2016), as well as with theoretical calculations that suggest a rather small vertical wavelength of the diurnal tide (Chapman & Lindzen, 1970). However, the semi-diurnal tide is more sensitive to the global atmospheric aerosol loading due to its long vertical wavelength and meridionally-broad nature. The semi-diurnal tide pattern is very similar compared to the diurnal tide, except for a much smaller amplitude. This suggests that the dust optical depth measured by Mastcam is largely representative of the global average, as was also found by Guzewich et al. (2016). The effect of atmospheric dust loading on the higher harmonics (ter-diurnal and quad-diurnal components) is slightly less studied. Results for the Perseverance (Sánchez-Lavega et al., 2023) indicate that column optical depth has some effect on the higher harmonics as well, but the effect is smaller compared to the diurnal and semi-diurnal components.

The amplitude patterns of both components observed by the InSight are extremely close to the patterns at the MSL location. There is, however, one clear difference: the amplitude of the diurnal component at the InSight location (average about 17 Pa) is much smaller compared to the MSL location (average about 33 Pa), which is in good agreement with Figures 1 (right panel) and 2. Similar peaks and drops in both components can be detected, therefore indicating that the local dust optical depths at the InSight location follow very nicely at least the pattern of the optical depths within the Gale Crater. Nevertheless, the amplitude of the semi-diurnal tide (average about 7 Pa) is very close to the amplitude observed by MSL (average about 10 Pa), due to the sensitivity of this component to global atmospheric dust loading. Hence, the absolute difference between

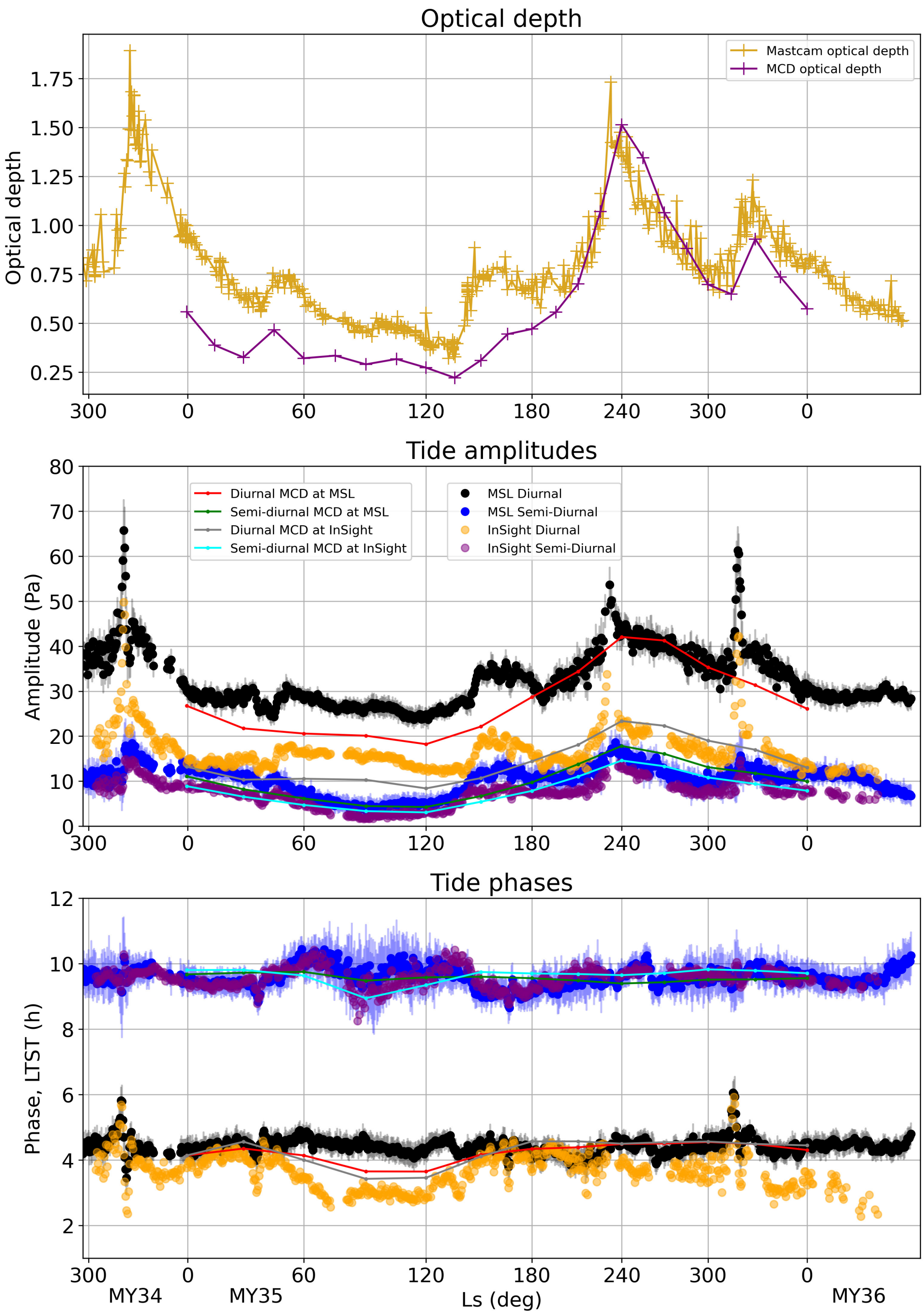

Figure 3. Mastcam optical depth as observed by MSL and daily mean dust column visible optical depth above surface from the MCD at the MSL location as a function of season (Ls) are shown in the upper panel. Middle panel shows diurnal and semi-diurnal tidal amplitudes (Pa) as observed by InSight and MSL as well as amplitudes obtained from the MCD. In addition, the estimated uncertainty for the MSL tidal components is shown. Bottom panel shows the corresponding tidal phases in hours (LTST).

the diurnal and semi-diurnal amplitudes at the InSight location is much smaller. For that reason, the semi-diurnal nature in the diurnal pressure cycles was also seen much easier in the InSight's diurnal pressure cycle in Figure 2.

The semi-diurnal component is, nevertheless, slightly smoother compared to the diurnal component at both stations. For example, the diurnal amplitude exhibits a big drop after a strong peak at the end of MY 34, but the semi-diurnal amplitude decreases smoothly after its peak. Therefore, the rapid drop in the diurnal component is likely due to local variations in dust optical depth. Near MY 35 Ls 180°, a drop in the dust optical depth is also visible. This drop is not seen at all in the semi-diurnal component, but a clear drop, of about 5 Pa, is seen in the diurnal component.

Previous work has also reported the sensitivity of the tides to water ice aerosol loading (Wilson & Guzewich, 2014; Kleinböhl et al., 2013), but results in Guzewich et al. (2016) suggest that dust is the dominant component for the tide variability within the Gale during MY 32. During the aphelion cloud belt season (about Ls 40–140°), the sky above the Gale is usually cloudless (Moores et al., 2015). During the same time period MSL and InSight (Figure 3 middle panel) both observed their lowest amplitudes for the diurnal and semi-diurnal components. The semi-diurnal amplitude steadily decreases from about Ls 50° to about Ls 90° for both stations, although the amount of water ice clouds increases (e.g. Smith, 2004; Khayat et al., 2023). Therefore, the decrease in the semi-diurnal amplitude is caused by the decrease in dust storm activity during the aphelion season.

The dust events in Figure 3 upper panel at about Ls 230° in MY 35 and at Ls 320° in both MY 34 and MY 35 are regional-scale or planet encircling Southern Hemisphere dust storms and they are identified as 'A' and 'C' dust storms (Kass et al., 2016). These two seasonal storms are regular and quite similar but 'C' storms have more annual variation. These specific dust storm events are also visible as peaks in the diurnal tide amplitude (Figure 3 middle panel) as well as in the diurnal range of pressure (Figure 1, right). Furthermore, the fast increase in optical depths around Ls 150° is captured by the diurnal range of pressure and amplitude of the diurnal tide.

The effect of the Ls 230° and Ls 320° dust events is also clearly visible in Figure 4, which shows the daily pressure cycles 13 sols before (black) and during (blue) the events for the InSight. It should be noted that the highest Mastcam optical depths were observed at about Ls 232° and Ls 328°, but the highest diurnal amplitudes for the InSight occurred at about Ls 230° and Ls 319°. The diurnal range of pressure increases substantially from about 50 to 80 Pa by the Ls 230° (Figure 4 left) event and from about 44 to 94 Pa by the Ls 320° (Figure 4 right) event. In addition, the extreme values of the sol are slightly shifted. During the both dust events, both extreme values are observed earlier than before the storm. For the Ls 230° dust event, the maximum and minimum pressures before the storm are observed at 07:38 and 17:08 LTST, while the values during the storm are observed at 07:07 and 16:55 LTST. The corresponding shifts for the Ls 320° dust event are from 07:16 to 06:15 LTST for the maximum pressure and from 16:49 to 16:37 LTST for the minimum pressure. Therefore, the shift of the diurnal pressure cycle is much higher during the Ls 320° dust event, which is also visible in the phase of the diurnal cycle (Figure 3 lower panel).

The phase of the diurnal tide at the InSight location has substantially more variability compared to the MSL (Figure 3 lower panel). The phase at the InSight location is generally 02:30–04:30 LTST (average of 03:39 LTST), with the minimum of about 02:16 LTST. In the diurnal phase, InSight observed a phase advance (maximum occurring earlier in the day) near MY 36 Ls 0–30°, while the opposite occurred one year earlier. Interestingly, this feature does not appear to be due to behavior in the tidal amplitudes, as Figure 3 middle panel show relatively similar behavior for these two periods. Another interesting feature is the wide drop in the phase at MY 35 Ls 30–180°, which is not seen at the MSL location. This may be related to the interaction of the diurnal Kelvin wave

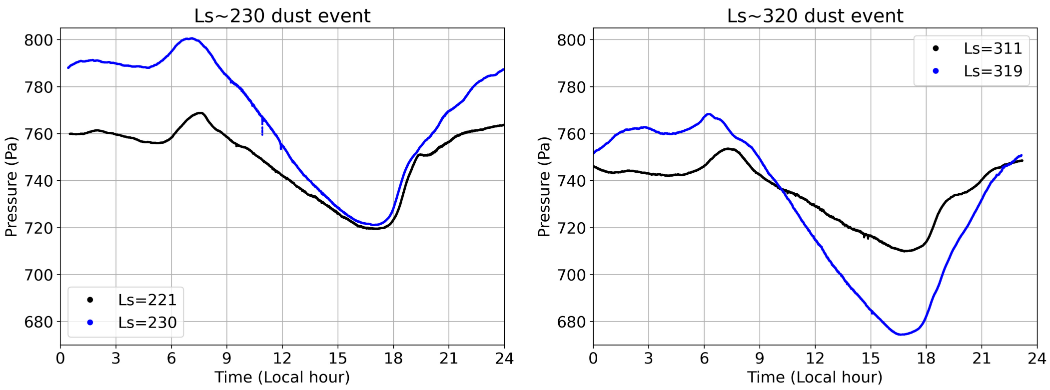

Figure 4. Diurnal pressure cycles before (black) and during (blue) the MY 35 Ls 230° (left) and Ls 320° (right) dust events.

and sun-synchronous wave, since Kelvin wave is expected to be strongest during the solstice seasons (Ls 90˚) (e.g. Guzewich et al., 2016). Furthermore, the diurnal Kelvin wave phase simulated over a full year seems to reach a minimum at this time of the year (Fig. 20, Wilson & Hamilton, 1996).

The phase of the diurnal tide at the MSL location (Figure 3 lower panel) is typically 04–05 LTST (average of 04:25 LTST), with couple exceptions. Two clear peaks in the phase are easily seen at approximately Ls 315˚ in MY 34 and MY 35 like observed in Zurita-Zurita et al. (2022). Same peaks are additionally visible at the InSight location, but they are slightly more pronounced. Their timing corresponds to the amplitude peaks seen in Figure 3 middle panel. One interesting feature is the phase just before MY 35 Ls 240˚. The diurnal tide phase excursion is much smaller compared to the two clear peaks, although a clear spike in amplitude is observed at that time of the year.

The semi-diurnal tide phase at both locations typically varies between 09 and 10 LTST, with averages of 09:34 and 09:36 LTST for InSight and MSL, respectively (Figure 3 lower panel). Both stations observe two sharp drops, located near MY 35 Ls 36˚ and Ls 165˚. On top of that, MSL observes a third sharp drop near MY 35 Ls 260˚, which is not visible in the InSight's measurements. All these semi-diurnal tide phase drops also appear as sharp drops in the diurnal tide phase. In addition to this, both stations detect drops in diurnal and semi-diurnal amplitudes near MY 35 Ls 36˚ and Ls 165˚. However, MSL does not observe amplitude drops near MY 35 Ls 260˚. These amplitude drops and peaks around MY 35 Ls 36˚ are likely related to a rare large-scale regional dust event that occurred at about Ls 35–50˚(Kass et al., 2022).

These two weather stations are located very close together, (4.5 ˚N, 135.6 ˚E) and (4.6 ˚S, 137.4 ˚E) for InSight and MSL, respectively. Due to almost the same longitude, both of them have synchronous solar forcing and hence that should not contribute to the apparent difference with the diurnal phases (Figure 3 lower panel) between these platforms. A slightly different interaction between the diurnal Kelvin wave and sun-synchronous wave may cause this difference.

The uncertainty in MSL tidal amplitudes estimated by a Monte Carlo analysis is on average less than 3 Pa around the measured values. The estimated uncertainty for the phases are around 19 and 33 minutes for the diurnal and semi-diurnal components, respectively. These estimations in MSL analysis represents sort of maximum range of uncertainty, as our approach estimates the uncertainty as a half of the difference between the maximum and minimum pressures for each hour. This uncertainty describes the situation if the measurement is at the start or end of the hour. Therefore, the uncertainty is much lower than that for the most of the hours as the timestamp is somewhere between. These uncertainties for the InSight are much smaller due to almost continuous data sampling. Thus, the mean calculated for each hour does not have the same issue as for the MSL, as MSL may have observations for example only at the first half of the hour. Therefore, we decided not to make uncertainty estimates for the tidal components of the InSight.

The amplitude of the diurnal tide obtained from the MCD mimics the observations relatively well at both weather stations. Nonetheless, the diurnal amplitude from the MCD is slightly lower than the observed at both locations during MY 35 Ls 0–180°. Average differences between the observed and MCD diurnal amplitudes during this time period are about 4.6 Pa and 6.8 Pa for InSight and MSL, respectively. This feature is very likely related to local/regional atmospheric dust loading. The daily mean dust column visible optical depth above surface obtained from the MCD is lower than the Mastcam observed dust optical depth during MY 35 Ls 0–180°, while the optical depths from the MCD match nicely to observed ones after that (Figure 3 upper panel). The semi-diurnal tide amplitude from the MCD mimics the observations even better, as expected, since this mode is sensitive to the global atmospheric dust loading, which is much more accurately described in the MCD.

The diurnal tide phase from the MCD follows quite nicely the phase derived from the MSL observations, but the MCD phase at the InSight location is about half an hour ahead throughout MY 35. However, the shape of the diurnal tide phase from the MCD is really close to the measured shape. At both stations, the semi-diurnal phases from the MCD are close to those observed, but much less variation.

Changing a one sol window to a window of three sols had very small effect. The average of the diurnal phase of InSight changed from 03:39 to 03:37 LTST and the minimum value for the diurnal phase of the InSight changed from 02:16 to 02:07 LTST. Also the amplitude peaks were slightly lower.

5 Summary and Discussion

Martian equatorial pressure observations by the InSight and the Mars Science Laboratory (MSL) were used to determine the sol-averaged and diurnal range of pressure during Martian year (MY) 35. The familiar CO_2 cycle and similar patterns of diurnal pressure range were displayed at both weather stations. Nonetheless, the amplitude of the diurnal pressure range was much higher at the MSL location due to the thermo-topographic lateral hydrostatic adjustment flow generated by the topography (Richardson & Newman, 2018). The same features were seen in the diurnal pressure cycles, but they additionally showed the dominance of the pressure wave with a period of 24 hours at both observing platforms.

Atmospheric tidal components, diurnal and semi-diurnal, were further analyzed by a fast Fourier transform (FFT) from simultaneous InSight and MSL pressure observations for more than one MY. The amplitude of the diurnal component was the largest at both weather stations during the analysis period and it also clearly demonstrated its sensitivity to the local atmospheric dust loading. The patterns of the semi-diurnal component at both platforms were similar to those of the diurnal component, except that the semi-diurnal component was smoother. The average amplitude of the semi-diurnal component was 7 Pa and 10 Pa for InSight and MSL, respectively.

This and many previous studies (e.g. Zurek, 1976; C. B. Leovy, 1981; Wilson & Hamilton, 1996) have shown the effect of the atmospheric dust loading on the amplitude of the diurnal and semi-diurnal components. However, in the future it would be useful to study how optical depths also affect higher harmonics (especially ter-diurnal component). This property was tested for the Perseverance (Sánchez-Lavega et al., 2023) and the results suggest that the column optical depth (dust and clouds) has some effect on the higher harmonics as well.

One clear difference between the weather stations was the average amplitude of the diurnal component, which was 17 Pa and 33 Pa at the InSight and MSL locations, respectively. The lateral hydrostatic adjustment flow, which is generated by the topography within the Gale Crater, increases the amplitude of the diurnal pressure range and therefore additionally the diurnal tide amplitude. The interaction of the sun-synchronous tide with the Kelvin wave may also be a factor, since results from the MarsWRF general circulation model (Guzewich et al., 2016) suggest that the diurnal Kelvin wave amplifies the amplitude of the diurnal tide within the Gale Crater. Due to the relatively close location, we expect a fairly similar effect on Elysium Planitia. However, the strength of the effect may vary due to topographical differences between the locations. This cannot yet be studied with in-situ observations, as single observing platform or two platforms with nearly the same longitude cannot distinguish between eastward and westward propagating waves.

The phase of the diurnal tide at the InSight location was generally lower than that at the MSL location, with averages of 03:39 LTST and 04:25 LTST. Moreover, MSL observed relatively constant diurnal tide phase while InSight detected much more variation. Both stations observed two distinct peaks near Ls 315° in MY 34 and MY 35. These peaks correspond to the timing of the diurnal tide amplitude peaks and high dust optical depth values. Interestingly, one amplitude peak was, however, not detected by the diurnal tide phase at either stations. Furthermore, InSight captured a wide drop in the diurnal phase at MY 35 Ls 30–180°, which was not seen by the MSL. The diurnal Kelvin wave is expected to be the strongest during the solstice seasons (Guzewich et al., 2016). Therefore, the interaction of the sun-synchronous component with the Kelvin wave may be related to this phase behavior. The pattern of the semi-diurnal phase was, on the other hand, very similar at both stations with averages of 09:34 and 09:36 LTST for InSight and MSL, respectively.

In the FFT analysis, we used hourly binned data. The InSight lander generally measured continuously, therefore the hourly averaged data is a good representation of the measured diurnal pressure cycle. The hourly binned data for MSL is, however, not so evenly spaced. When combining the data into one hour bins, we assumed that the timestamp is in the middle of the hour. This causes some errors when calculating the amplitudes and phases of the tidal components. A Monte Carlo analysis provided estimates for the maximum range of uncertainty for the MSL tidal components. On average, amplitudes varied less than 3 Pa around the observed amplitudes. The estimated uncertainty for the phases were around 19 and 33 minutes for the diurnal and semi-diurnal components, respectively. Therefore, these uncertainties were not calculated for the InSight due to the continuous measurement strategy.

The amplitude of the diurnal tide obtained from a Mars Climate Database (MCD) mimicked the observations quite well at both locations, except during MY 35 Ls 0–180°. The amplitude obtained from the MCD was slightly lower than the observed amplitudes. This is very likely explained by the atmospheric dust conditions, since the diurnal tide is sensitive to the local atmospheric dust loading. The dust optical depth obtained from the MCD was lower than the Mastcam observed optical depth during this period, but was in good agreement with observations during MY 35 Ls 180–360°. The amplitude of the semi-diurnal tide is sensitive to global atmospheric dust loading, and hence the amplitude from the MCD nicely mimicked the observed one.

This study shows that atmospheric tides dominate the daily surface pressure variations in the Martian tropics. Two simultaneously observing surface platforms are extremely beneficial for studying the dynamics of the Martian atmosphere. Together with model simulations, an even larger number of in-situ measurement stations around the planet would help us to improve our knowledge on the influence of location, topography and surface properties on these tides.

Open Research Section

MSL (PDS3 format) and InSight (PDS4 format) pressure data are freely available from the Planetary Data System Atmospheres Node (Gomez-Elvira, 2013; Banfield et al., 2019). Atmospheric optical depths are retrieved from MSL Mastcam solar tau imaging sequences following the methodology of Lemmon et al. (2015) and values used in this study are available on Leino et al. (2023). Meteorological fields from the Mars Climate Database are available at `http://www-mars.lmd.jussieu.fr/mcd_python/` (Forget et al., 1999; Millour et al., 2017). Derived data products analyzed and presented in the manuscript are available on Leino et al. (2023).

Acknowledgments

Joonas Leino, Mark Paton and Ari-Matti Harri are thankful for the Finnish Academy grant number 310509. This research was carried out at the Jet Propulsion Laboratory, California Institute of Technology, under a contract with the National Aeronautics and Space Administration (80NM0018D0004). The JPL co-authors acknowledge funding from NASA's Space Technology Mission Directorate and the Science Mission Directorate.

References

Banfield, D., Conrath, B., Pearl, J. C., Smith, M. D., & Christensen, P. (2000). Thermal tides and stationary waves on mars as revealed by mars global surveyor thermal emission spectrometer. *Journal of Geophysical Research: Planets*, *105*(E4), 9521-9537. doi: https://doi.org/10.1029/1999JE001161

Banfield, D., Mora Sotomayor, L., & Huber, L. (2019). *Insight auxiliary payload sensor subsystem (apss) pressure sensor (ps) archive bundle* [dataset]. doi: https://doi.org/10.17189/1518939

Bridger, A. F. C., & Murphy, J. R. (1998). Mars' surface pressure tides and their behavior during global dust storms. *Journal of Geophysical Research: Planets*, *103*(E4), 8587-8601. doi: https://doi.org/10.1029/98JE00242

Chapman, S., & Lindzen, R. (1970). *Atmospheric tides* (Vol. 10). doi: 10.1007/BF00171584

Forget, F., Hourdin, F., Fournier, R., Hourdin, C., Talagrand, O., Collins, M., ... Huot, J.-P. (1999, October). Improved general circulation models of the Martian atmosphere from the surface to above 80 km. *Journal of Geophysical Research, Volume 104, Issue E10, p. 24155-24176*, *104*(E10), 24155-24176. doi: 10.1029/1999JE001025

Gómez-Elvira, J., Armiens, C., Castañer, L., Domínguez, M., Genzer, M., Gómez, F., ... Martín-Torres, J. (2012, August). REMS: The Environmental Sensor Suite for the Mars Science Laboratory Rover. *Space Sci. Rev.*, *170*(1-4), 583-640. doi: 10.1007/s11214-012-9921-1

Gomez-Elvira, J. (2013). *Mars science laboratory rover environmental monitoring station rdr data v1.0, msl-m-rems-5-modrdr-v1.0, nasa planetary data system* [dataset]. doi: https://doi.org/10.17189/1523033

Guzewich, S. D., Newman, C., de la Torre Juárez, M., Wilson, R., Lemmon, M., Smith, M., ... Harri, A.-M. (2016). Atmospheric tides in gale crater, mars. *Icarus*, *268*, 37-49. Retrieved from `https://www.sciencedirect.com/science/article/pii/S0019103515005850` doi: https://doi.org/10.1016/j.icarus.2015.12.028

Hagan, M. E., & Roble, R. G. (2001). Modeling diurnal tidal variability with the national center for atmospheric research thermosphere-ionosphere-mesosphere-electrodynamics general circulation model. *Journal of Geophysical Research: Space Physics*, *106*(A11), 24869-24882. doi: https://doi.org/10.1029/2001JA000057

Hamilton, K. (1982). The effect of solar tides on the general circulation of the martian atmosphere. *Journal of Atmospheric Sciences*, *39*(3), 481 - 485. doi: 10.1175/1520-0469(1982)039⟨0481:TEOSTO⟩2.0.CO;2

Harri, A.-M., Genzer, M., Kemppinen, O., Kahanpää, H., Gomez-Elvira, J., Rodriguez-Manfredi, J. A., ... the REMS/MSL Science Team (2014). Pressure observations by the curiosity rover: Initial results. *Journal of Geophysical Research: Planets*, *119*(1), 82-92. doi: 10.1002/2013JE004423

Harri, A. M., Marsal, O., Lognonne, P., Leppelmeier, G. W., Spohn, T., Glassmeier, K. H., ... Tillman, J. E. (1999, January). Network science landers for Mars. *Advances in Space Research*, *23*(11), 1915-1924. doi: 10.1016/S0273-1177(99)00279-3

Karlgaard, C. D., Korzun, A. M., Schoenenberger, M., Bonfiglio, E. P., Kass, D. M., & Grover, M. R. (2021). Mars insight entry, descent, and landing trajectory and atmosphere reconstruction. *Journal of Spacecraft and Rockets*, *58*(3), 865-878. Retrieved from `https://doi.org/10.2514/1.A34913` doi: 10.2514/1.A34913

Kass, D. M., Kleinboehl, A., Shirley, J. H., Cantor, B. A., & Heavens, N. G. (2022, December). Observations of the Mars Year 35 E (Early) Large-Scale Regional Dust Event. In *Agu fall meeting abstracts* (Vol. 2022, p. P32B-02).

Kass, D. M., Kleinböhl, A., McCleese, D. J., Schofield, J. T., & Smith, M. D. (2016). Interannual similarity in the martian atmosphere during the dust storm season. *Geophysical Research Letters*, *43*(12), 6111-6118. Retrieved from `https://agupubs.onlinelibrary.wiley.com/doi/abs/10.1002/2016GL068978` doi: https://doi.org/10.1002/2016GL068978

Khayat, A. S. J., Smith, M. D., Wolff, M. J., Guzewich, S. D., Mason, E. L., & Atwood, S. (2023). The mars atmosphere water ice aerosol climatology by mro/crism: 5 mars years of observations. *Journal of Geophysical Research: Planets*, *128*(7), e2023JE007761. Retrieved from `https://agupubs.onlinelibrary.wiley.com/doi/abs/10.1029/2023JE007761` (e2023JE007761 2023JE007761) doi: https://doi.org/10.1029/2023JE007761

Kleinböhl, A., John Wilson, R., Kass, D., Schofield, J. T., & McCleese, D. J. (2013). The semidiurnal tide in the middle atmosphere of mars. *Geophysical Research Letters*, *40*(10), 1952-1959. doi: https://doi.org/10.1002/grl.50497

Leino, J., Harri, A.-M., Banfield, D., de la Torre Juárez, M., Paton, M., Rodriguez-Manfredi, J.-A., ... Savijärvi, H. (2023). *Derived data products analyzed and presented in the manuscript "martian equatorial atmospheric tides from surface observations".* [dataset]. Finnish Meteorological Institute. Retrieved from `https://fmi.b2share.csc.fi/records/0a1064b916584621bc1fe6ea86c92e02` doi: 10.23728/FMI-B2SHARE.0A1064B916584621BC1FE6EA86C92E02

Lemmon, M. T. (2014, July). The Mars Science Laboratory Optical Depth Record. In *Eighth international conference on mars* (Vol. 1791, p. 1338).

Lemmon, M. T., Wolff, M. J., Bell, J. F., Smith, M. D., Cantor, B. A., & Smith, P. H. (2015). Dust aerosol, clouds, and the atmospheric optical depth record over 5 mars years of the mars exploration rover mission. *Icarus*, *251*, 96-111. Retrieved from `https://www.sciencedirect.com/science/article/pii/S0019103514001559` (Dynamic Mars) doi: https://doi.org/10.1016/j.icarus.2014.03.029

Leovy, C., & Zurek, R. (1979, 07). Thermal tides and martian dust storms - direct evidence for coupling. *J. Geophys. Res.*, *84*. doi: 10.1029/JB084iB06p02956

Leovy, C. B. (1981). Observations of martian tides over two annual cycles. *Jour-*

nal of Atmospheric Sciences, *38*(1), 30 - 39. doi: 10.1175/1520-0469(1981)038⟨0030:OOMTOT⟩2.0.CO;2

Martínez, G. M., Newman, C. N., De Vicente-Retortillo, A., Fischer, E., Renno, N. O., Richardson, M. I., . . . Vasavada, A. R. (2017, October). The Modern Near-Surface Martian Climate: A Review of In-situ Meteorological Data from Viking to Curiosity. *Space Sci rev*, *212*(1-2), 295-338. doi: 10.1007/s11214-017-0360-x

Millour, E., Forget, F., Spiga, A., Vals, M., Zakharov, V., Navarro, T., . . . MCD/GCM Development Team (2017). The Mars Climate Database (MCD version 5.3). In *Egu general assembly conference abstracts* (p. 12247).

Moores, J. E., Lemmon, M. T., Rafkin, S. C., Francis, R., Pla-Garcia, J., de la Torre Juárez, M., . . . McCullough, E. (2015). Atmospheric movies acquired at the mars science laboratory landing site: Cloud morphology, frequency and significance to the gale crater water cycle and phoenix mission results. *Advances in Space Research*, *55*(9), 2217-2238. Retrieved from https://www.sciencedirect.com/science/article/pii/S0273117715001015 doi: https://doi.org/10.1016/j.asr.2015.02.007

Richardson, M. I., & Newman, C. E. (2018). On the relationship between surface pressure, terrain elevation, and air temperature. part i: The large diurnal surface pressure range at gale crater, mars and its origin due to lateral hydrostatic adjustment. *Planetary and Space Science*, *164*, 132-157. Retrieved from https://www.sciencedirect.com/science/article/pii/S0032063316301878 doi: https://doi.org/10.1016/j.pss.2018.07.003

Savijärvi, H., Crisp, D., & Harri, A.-M. (2005). Effects of co2 and dust on present-day solar radiation and climate on mars. *Quarterly Journal of the Royal Meteorological Society*, *131*(611), 2907-2922. Retrieved from https://rmets.onlinelibrary.wiley.com/doi/abs/10.1256/qj.04.09 doi: https://doi.org/10.1256/qj.04.09

Smith, M. D. (2004). Interannual variability in tes atmospheric observations of mars during 1999–2003. *Icarus*, *167*(1), 148-165. Retrieved from https://www.sciencedirect.com/science/article/pii/S0019103503002872 (Special Issue on DS1/Comet Borrelly) doi: https://doi.org/10.1016/j.icarus.2003.09.010

Spiga, A., Banfield, D., Teanby, N. A., Forget, F., Lucas, A., Kenda, B., . . . Banerdt, W. B. (2018, October). Atmospheric Science with InSight. *Space Science Reviews*, *214*(7), 109. doi: 10.1007/s11214-018-0543-0

Spiga, A., Murdoch, N., Lorenz, R., Forget, F., Newman, C., Rodriguez, S., . . . Banerdt, W. B. (2021). A study of daytime convective vortices and turbulence in the martian planetary boundary layer based on half-a-year of insight atmospheric measurements and large-eddy simulations. *Journal of Geophysical Research: Planets*, *126*(1), e2020JE006511. Retrieved from https://agupubs.onlinelibrary.wiley.com/doi/abs/10.1029/2020JE006511 (e2020JE006511 2020JE006511) doi: https://doi.org/10.1029/2020JE006511

Squyres, S. W. (1995, April). The Mars environmental survey (mesur) mission. *Advances in Space Research*, *15*(4), 179-188. doi: 10.1016/0273-1177(94)00079-G

Sánchez-Lavega, A., del Rio-Gaztelurrutia, T., Hueso, R., Juárez, M. d. l. T., Martínez, G. M., Harri, A.-M., . . . Mäkinen, T. (2023). Mars 2020 perseverance rover studies of the martian atmosphere over jezero from pressure measurements. *Journal of Geophysical Research: Planets*, *128*(1), e2022JE007480. Retrieved from https://agupubs.onlinelibrary.wiley.com/doi/abs/10.1029/2022JE007480 (e2022JE007480 2022JE007480) doi: https://doi.org/10.1029/2022JE007480

Vasavada, A. R., Grotzinger, J. P., Arvidson, R. E., Calef, F. J., Crisp, J. A., Gupta, S., . . . Yingst, R. A. (2014). Overview of the mars science laboratory mission: Bradbury landing to yellowknife bay and beyond. *Journal of Geophysical Research: Planets*, *119*(6), 1134-1161. Retrieved from https://agupubs.onlinelibrary.wiley.com/doi/abs/10.1002/2014JE004622 doi: https://doi.org/10.1002/2014JE004622

Wilson, R. J., & Guzewich, S. D. (2014). Influence of water ice clouds on nighttime tropical temperature structure as seen by the mars climate sounder. *Geophysical Research Letters*, *41*(10), 3375-3381. Retrieved from https://agupubs.onlinelibrary.wiley.com/doi/abs/10.1002/2014GL060086 doi: https://doi.org/10.1002/2014GL060086

Wilson, R. J., & Hamilton, K. (1996). Comprehensive model simulation of thermal tides in the martian atmosphere. *Journal of Atmospheric Sciences*, *53*(9), 1290 - 1326. doi: 10.1175/1520-0469(1996)053⟨1290:CMSOTT⟩2.0.CO;2

Zurek, R. (1976, 03). Diurnal tide in the martian atmosphere. *Journal of the Atmospheric Sciences*, *33*. doi: 10.1175/1520-0469(1976)033⟨0321:DTITMA⟩2.0.CO;2

Zurita-Zurita, S., de la Torre Juárez, M., Newman, C. E., Viúdez-Moreiras, D., Kahanpää, H. T., Harri, A.-M., ... Rodríguez-Manfredi, J. A. (2022). Mars surface pressure oscillations as precursors of large dust storms reaching gale. *Journal of Geophysical Research: Planets*, *127*(8), e2021JE007005. Retrieved from https://agupubs.onlinelibrary.wiley.com/doi/abs/10.1029/2021JE007005 (e2021JE007005 2021JE007005) doi: https://doi.org/10.1029/2021JE007005